ISSN : 2231-0711

NUC Algorithm for Correcting Gain and Offset Non-uniformities

Parul Goyal
Department of Electronics & Communication Engineering
Dev-Bhoomi Institute of Technology, Dehradun - 248001, Uttarakhand, India
Research Scholar, Singhania University, Pacheri Bari, Dist. Jhunjhunu-333515, Rajasthan, India
Email parulgoya2007@yahoo.com

Abstract-This paper describes a model for gain and offset non-uniformities and correction algorithm for non-uniformities. The infrared sensor model determines the number of photoelectrons generated from total incident flux and relates these electrons with integration time. It includes gain and offset non-uniformities in infrared sensor. A methodology for calibrating the sensor non-uniformities is presented. The uncorrected infrared data is collected by exposing the infrared sensor against a very high emissive source such as black body or sky. This data is then used for sensor calibration. This algorithm is tested on cooled infrared imaging system. The results show that residual non-uniformities are reduced from 6% to less that 0.6% after performing the correction. Further, it is observed that the system is fully calibrated at two calibration points. The spatial noise after non-uniformity correction is compared with the temporal noise of the system and the results illustrates that the spatial noise is reduced significantly lower than the temporal noise of the system. This approach offers the upgradeability of gain and offset coefficients, thus making the system more robust by giving same performance under all environmental conditions.

1. INTRODUCTION

1.1 Infrared Sensor Model

Infrared sensor model that maps the focal plane array onto the object space is shown in Fig. 1.

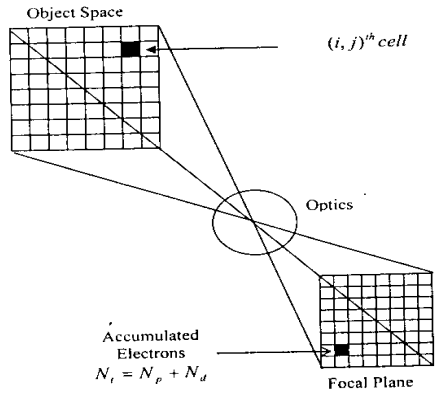

Figure 1 Schematic for IR Sensor model

It expresses the output of an arbitrary (i, j)th pixel in terms of the number of electrons accumulated at the pixel over the integration time. The number of photoelectrons accumulated at (i, j)th pixel during the integration time is given by

$$N_{ij} = \tau_0 T_{int} \int_{\lambda_1}^{\lambda_2} \eta_{ij} \left[\varepsilon_{ij}(\lambda) . L(\lambda, T_{ij}) + \{1 - \varepsilon_{ij}(\lambda)\} . L(\lambda, T_b) \right] . A_{ij} . \Omega_{ij} . d\lambda \quad \ldots\ldots\ldots\ldots (1.1)$$

Where $L(\lambda,T_{ij})$ is the photon radiance as a function of the wavelength for (i, j)th cell in the object space and $L(\lambda,T_b)$ is the ambient photon radiance for the background. Plank's law gives the photon radiance of the object as a function of wavelength and temperature and is defined as

$$L(\lambda, Tij) = \frac{2\pi c}{\lambda^4 \exp\left(\frac{hc}{\lambda kT}\right) - 1} \quad \ldots\ldots\ldots\ldots\ldots (1.2)$$

The term Ω_{ij} described in equation 1.1 is the projected solid angle as viewed from the FPA and is given as

$$\Omega_{ij} = \frac{\pi . \cos^4 \theta_{ij}}{1 + 4 (F/\#)^2} \quad \ldots\ldots\ldots\ldots (1.3)$$

ε_{ij} is the emissivity of the scene as a function of the wavelength averaged over the pixel and $\eta_{ij}(\lambda)$ is the quantum efficiency of the (i, j)th pixel as a function of the wavelength. The term [1-$\varepsilon_{ij}(\lambda)$] is the reflectivity of the scene as a function of the wavelength averaged over the pixel. It is included to account that each pixel of the object space is not only emitting, but also reflecting as well. The remaining terms from the above equations are defined as follows. F/# is the f-number of the optics, A_{ij} is the pixel active area, τ_0 is the effective transmittance of the optical system, θ_{ij} is the pixel angular displacement from optical axis. λ_1 and λ_2 are the lower and upper cutoff wavelengths of the optical system respectively, T_{int} is the integration time and c is the speed of light (=3.10^8 m/s). The cosine term represents the systematic variation of pixel illumination with position of the focal plane.

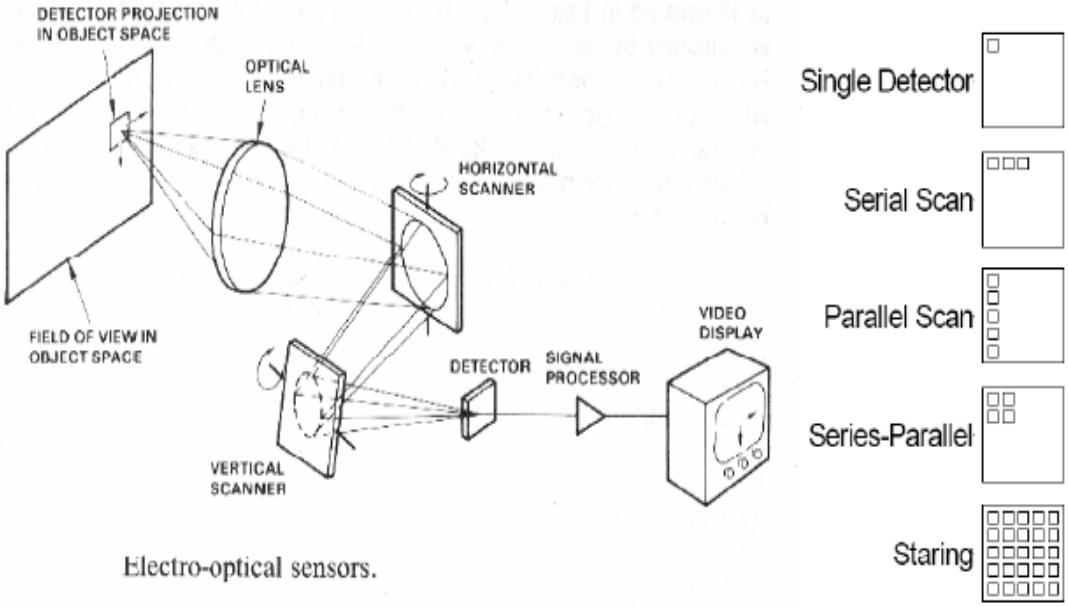

Figure 2 Read out Mode of a Focal Plane Array

Figure 2 illustrates the Read out Mode of a Focal Plane Array. Dark charge will also accumulate at each pixel. The dark charge is proportional to $e^{(-Eg/2KT)}$, where E_g is the band gap of the sensor material and T is absolute temperature ^{0}K. In general the amount of dark charge is also non-uniform from pixel to pixel. Thus the total number of electrons accumulated at (i, j) th pixel is

$$N_{ij} = \tau_0 T_{inc} \int_{\lambda_1}^{\lambda_2} \eta_{ij} \left[s_{ij}(\lambda) \cdot L(\lambda, T_{ij}) + \{1 - s_{ij}(\lambda)\} \cdot L(\lambda, T_b) \right] \cdot A_{ij} \cdot \Omega_{ij} \cdot d\lambda + N^d_{ij}$$

…….(1.4)

Defining the response coefficient R_{ij} by

$$R_{ij} = \tau_0 T_{inc} \cdot A_{ij} \cdot \Omega_{ij} = \tau_0 T_{inc} \left[\frac{\pi \cdot \cos^4 \theta_{ij}}{1 + 4 (F/\#)^2} \right] A_{ij} \quad \text{…. (1.5)}$$

Equation (3.4) may be written as

$$\langle \bar{N}_{ij} \rangle = \langle R_{ij} \cdot \int_{\lambda_1}^{\lambda_2} \eta_{ij} \{ s(\lambda) \overline{L(\lambda, T_s)} + [1 - s(\lambda)] \overline{L(\lambda, T_b)} \} \cdot d\lambda \rangle + \langle \bar{N}^d_{ij} \rangle$$

…….(1.6)

N^d_{ij} is the dark charge accumulated during the integration time. Fig. 3 shows the variation of the number of accumulated photoelectrons with ambient temperature at different integration times. Fig. 4 represents the variation of the number of accumulated photoelectrons with integration time at different ambient temperature.

Equations (1.4) and (1.6) describe the conversion of infrared radiations into visible image. In order to simplify the mathematical formulation it has been assumed that the response of the detector is linear in the incident photon flux. The effect of nonlinearity will be addressed later.

Fig. 3 shows the variation of the number of accumulated photoelectrons with ambient temperature at different integration times.

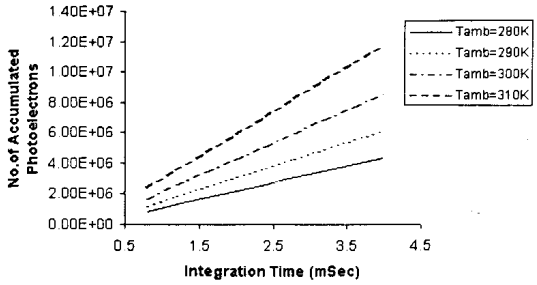

Fig 3

Fig. 4 represents the variation of the number of accumulated photoelectrons with integration time at different ambient temperature.

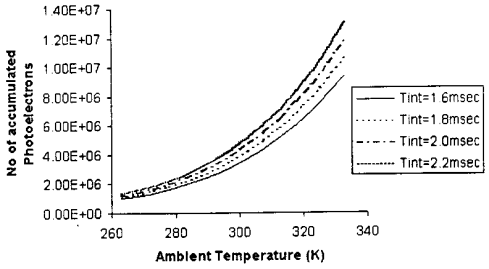

Fig 4

1.2 Model for Sensor Non-uniformities

Spatial noise at the output of a staring array sensor arises from random detector-to-detector photo response variations across the focal plane array. Additionally the imaging operation itself may introduce fixed pattern variations in the image. The offset non-uniformities are additive in nature, which arises from pixel to pixel variations in dark charge. Similarly the gain non-

uniformities are multiplicative in nature, which arises from spatial variations in the detector active area and its angular distance from optical axis. To analyze the impact of these non-uniformities, the output of a specific pixel is now described in term of its unique non-uniformities. We assume that the source is uniform and taking spatial and temporal averages of the total number of accumulated electrons across the array we obtain

$$\langle N_{ij} \rangle = \langle R_{ij} \int_{\lambda_1}^{\lambda_2} \eta_{ij} \{ \varepsilon(\lambda) L(\lambda, T_s) + [1 - \varepsilon_{ij}(\lambda)] L(\lambda, T_b) \} d\lambda \rangle + \langle N^d_{ij} \rangle$$

……..(1.7)

where T_s is the source temperature. We define

$$R_{ij} = \langle R_{ij} \rangle + r_{ij} \quad \text{…..(1.8)}$$

$$N^d_{ij} = \langle N^d_{ij} \rangle + \bar{n}^d_{ij} \quad \text{…..(1.9)}$$

$$\eta_{ij}(\lambda) = \langle \eta_{ij}(\lambda) \rangle + \kappa_{ij}(\lambda) \quad \text{….(1.10)}$$

The bracketed quantities $\langle R_{ij} \rangle$, $\langle N^d_{ij} \rangle$ and $\langle \eta_{ij}(\lambda) \rangle$ represent the spatial averages of the response coefficient, dark current and quantum efficiency respectively, taken over all pixels in the detector array. The quantities r_{ij}, $\bar{n}^d_{ij}$ and $\kappa_{ij}(\lambda)$ represent the incremental deviation (i, j) [th] pixel from mean value in response coefficient, dark current and quantum efficiency respectively. Substituting (1.7), (1.8), (1.9), (1.10) in (1.6) and taking the temporal average we arrive at:

$$\bar{N}_{ij} = \langle \bar{N}_{ij} \rangle + r_{ij} \int_{\lambda_1}^{\lambda_2} \langle \eta_{ij}(\lambda) \rangle \{ \varepsilon(\lambda) \overline{L(\lambda, T_s)} + [1 - \varepsilon(\lambda)] \overline{L(\lambda, T_b)} \} d\lambda + \bar{n}^d_{ij} + \langle R_{ij} \rangle \int_{\lambda_1}^{\lambda_2} \kappa_{ij}(\lambda) \{ \varepsilon(\lambda) \overline{L(\lambda, T_s)} + [1 - \varepsilon(\lambda)] \overline{L(\lambda, T_b)} \} d\lambda + r_{ij} \int_{\lambda_1}^{\lambda_2} \kappa_{ij}(\lambda) \{ \varepsilon(\lambda) \overline{L(\lambda, T_s)} + [1 - \varepsilon(\lambda)] \overline{L(\lambda, T_b)} \} d\lambda$$

…. (1.11)

The last integral in the above equation can be neglected as it is the product of two small terms r_{ij} and $\kappa_{ij}(\lambda)$. Thus (1.11) can be approximated by

$$\bar{N}_{ij} = \langle \bar{N}_{ij} \rangle + \frac{r_{ij}}{\langle R_{ij} \rangle} (\langle \bar{N}_{ij} \rangle - \langle N^d_{ij} \rangle) + \bar{n}^d_{ij} + \langle R_{ij} \rangle \int_{\lambda_1}^{\lambda_2} \kappa_{ij}(\lambda) \{ \varepsilon(\lambda) \overline{L(\lambda, T_s)} + [1 - \varepsilon(\lambda)] \overline{L(\lambda, T_b)} \} d\lambda \quad \text{….(1.12)}$$

It can be seen from equation (1.12) that if the spectral response of the pixel is uniform i.e. $\kappa_{ij}(\lambda)$=0 then a function involving only multiplication and addition can be used to correct the infrared imagery.

1.3 NUC Algorithm for calibrating the sensor non uniformities

An assumption is made that the IRFPA is exposed to a uniform source of IR radiations. The image of the scene generates a signal at each pixel that is proportional to local image incidence. The total current generated by the sensor element usually consists of the photon current, dark current and stray current. The stray current is due to Dewar stray emission and window stray emission and is generally negligible. The dark current is proportional to $e^{(-Eg/2KT)}$ where Eg is the band gap of the sensor material and T is the absolute temperature in ºK.

The output Yij of (i, j) [th] pixel is proportional to the number of photoelectrons accumulated at (i, j) th pixel during the integration time, as given by Equation 1.1. In order to perform the non-uniformity correction, sensor output is acquired by varying the integration time. Acquisition of sensor data by varying the integration time is equivalent to acquiring the data at artificially generated different temperature. The variation in number of photoelectrons due to change in integration time is equivalent to variation in number of photoelectrons due to two artificially generated temperatures. The integration time of the sensor is varied and the raw video data is acquired by exposing the system with a uniform and high emissivity source. To achieve this, first set of image data I1 is recorded at lower integration time and second set of image data I2 is recorded at higher integration time. Multiple frames of image, at each integration time, are recorded and averaged to reduce the temporal noise.

For the (i, j) [th] detector in the array, the measured signal Y_{ij} (detector response) is given by the following linear relationship.

$$Y_{ij} = a_{ij} X_{ij} + b_{ij} \quad \text{….(1.13)}$$

where G_{ij} and O_{ij} are the gain and offset non-uniformities associated with the (i, j)[th] detector pixel respectively and X_{ij} is the irradiance received by the (i, j)[th] detector pixel. Thus, after NUC correction, the above equation can be expressed as

$$X_{ij} = a'_{ij}(Y_{ij} - b_{ij}) \quad \text{…..(1.14)}$$

Where

$$a'_{ij} = \frac{1}{a_{ij}} \quad \text{…..(1.15)}$$

Defining

$$a'_{ij} = \frac{\langle I_2 \rangle - \langle I_1 \rangle}{I_{2ij} - I_{1ij}} \quad \text{….(1.16)}$$

$$b_{ij} = I_{1ij} \quad \text{….(1.17)}$$

where I_{1ij} and I_{2ij} are (i, j)[th] pixel intensities at lower and higher integration time, respectively. $\langle I_1 \rangle$ and $\langle I_2 \rangle$ are the spatial averages of the image frames at lower and higher integration time, respectively and are given as

$$\langle I_1 \rangle = \frac{1}{n1.n2} \sum_{i=1,j=1}^{n1,n2} I_{1ij} \quad \text{… (1.18)}$$

$$\langle I_2 \rangle = \frac{1}{n1.n2} \sum_{i=1,j=1}^{n1,n2} I_{2ij} \quad \text{…(1.19)}$$

where n1.n2 is the total number of pixels in a frame and m and n are number of rows and columns, respectively. Thus, from (4)–(9) the corrected output of the pixel (i, j) [th] is given as

$$X_{ij} = \frac{\langle I_2 \rangle - \langle I_1 \rangle}{I_{2ij} - I_{1ij}} (Y_{ij} - I_{1ij}) \quad \text{… (1.20)}$$

This algorithm can be further improved by taking in to account the higher order non-linear coefficients.

2. APPLICATIONS

The capability of non-uniformity correction algorithm can be evaluated by applying the algorithm on real infrared

data and studying the performance parameters. The infrared data is collected using 320 · 240 elements InSb staring focal plane array based cooled thermal imaging system operating in the 3–5 lm wavelength region. Thermal imaging system is designed based upon 50 mm optical aperture having f-number as F/3. The video processing electronic of thermal imaging system has been designed to perform non-uniformity correction, bad pixel replacement, digital scan conversion, automatic gain control and several image enhancement functions such as contrast enhancement and histogram equalization. Finally it generates CCIR standard video output at 50 Hz, which can be displayed on any monitor.

The image data is collected by varying the integration time of the sensor and exposing the infrared system to a high emissive source at uniform and constant temperature. Different sets of image data were captured at different integration times under different conditions. The integration time of the IRFPA is controlled through the video processing board. Two sets of image data are acquired at lower integration time of 2.0 ms and higher integration time of 2.4 ms, respectively. Eight frames of image data are collected at each integration time and averaged to reduce the temporal noise. This data is then used to compute the gain and offset coefficients. The integration time of thermal imaging system under normal operation is kept at 2.2 ms. The gain and offset corrections coefficients are then implemented on the incoming uncorrected image data. Figs. 5(a) and 5(b) show the image data obtained by exposing infrared system to a uniform source at lower and higher integration time, respectively.

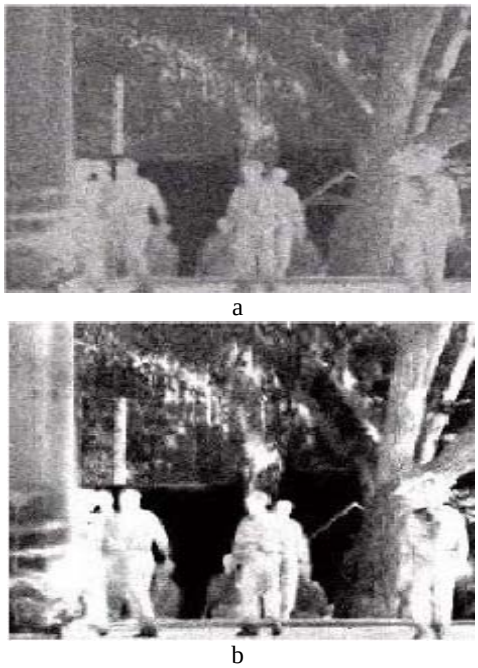

a

b

Fig. 5(a) Image data at lower integration time (b) Image data at higher integration time

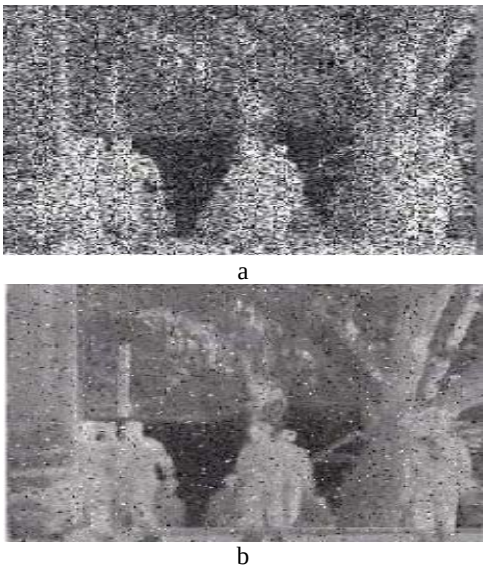

a

b

Fig. 6(a) Raw image data at 2.0 ms (b) Image data after NUC

Fig. 6(a) illustrates the image obtained with sensor non-uniformities at 2.0 msec integration time Fig. 6(b) illustrates the image data after non-uniformity correction. Fig. 7(a) and 7(b) represents the 3-D plots of the image data before and after non-uniformity correction. Over 100 IR image data frames with sensor non-uniformities have been acquired by operating the IRFPA at an integration time of 2.2 ms. The gain and offset coefficients calculated using the Fig. 5 is applied on these image frames.

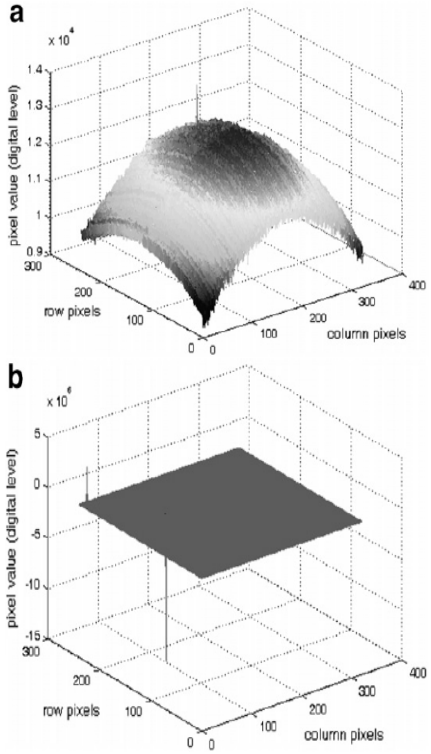

Fig. 7(a) 3D plot of raw image data (b) 3D plot of image data after NUC

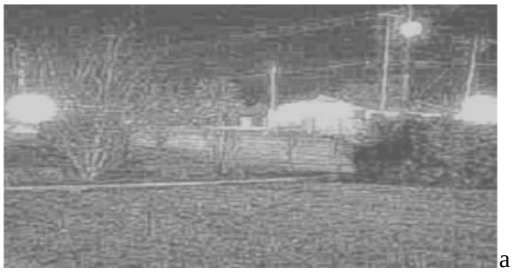

a

b

Fig. 8(a) Image frame before NUC (b) Image frame after NUC

a

b

Fig. 9(a) Image frame before NUC (b) Image frame after NUC

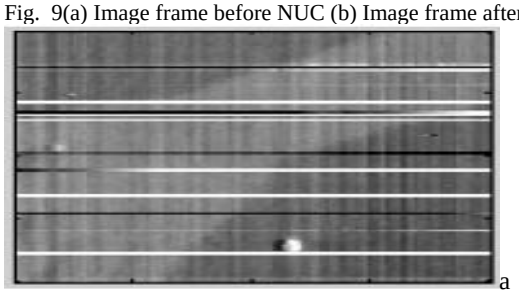

a

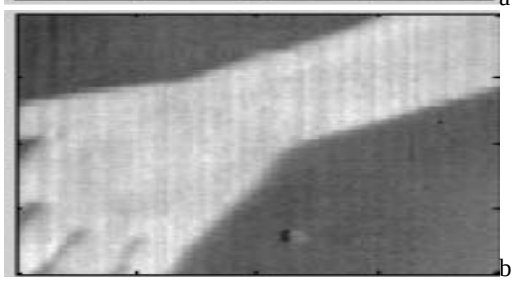

b

Fig. 10 (a) Image frame before NUC (b) Image frame after NUC

Figs. 8, 9 & 10 show the sample image frames with sensor non-uniformities and corrected image after performing non-uniformity correction.

3. PERFORMANCE EVALUATION

The performance of non-uniformity correction algorithm is evaluated by a correction parameter called as residual non-uniformity (RNU) which is defined as standard deviation (SD) of the corrected FPA signal divided by the mean signal (mean). Mathematically it can be expressed as

$$RNU = \frac{SD}{Mean} = \frac{1}{\bar{X}}\sqrt{\frac{1}{LxM}\sum_{i=1}^{L}\sum_{j=1}^{M}(X_{i,j}-\bar{X})^2} \quad \ldots (1.21)$$

where L and M are the dimensions of IRFPA, X_{ij} is the output of the pixel (i, j) and $\bar{X}$ is spatial mean of the pixels in the IRFPA, which is defined as

$$\bar{X} = \frac{1}{LxM}\sum_{i=1}^{L}\sum_{j=1}^{M}X_{i,j} \quad \ldots (1.22)$$

The performance of the algorithm was evaluated using a 320 · 240 elements InSb FPA based infrared imaging system. The FPA is integrated with Xilinx XC2V2000 FPGA based video processing board. This board generates various controls and clock signals for FPA and also changes the integration time of FPA. 14-bit analog to digital converter (AD9240 from Analog Device) is used to convert the video signal from FPA into digital form and then store into the memory. A PC based application was developed to control the various function of the video processing board through serial link and capture the digital data.

One set of data was captured by exposing the infrared system with a uniform source at 30 ºC temperature. Another set of data was captured at 17 ºC temperature. The non-uniformities were computed for the uncorrected data and corrected data and the plots of RNU (%) with integration time at 30 ºC and 17 ºC are given in Fig.11.

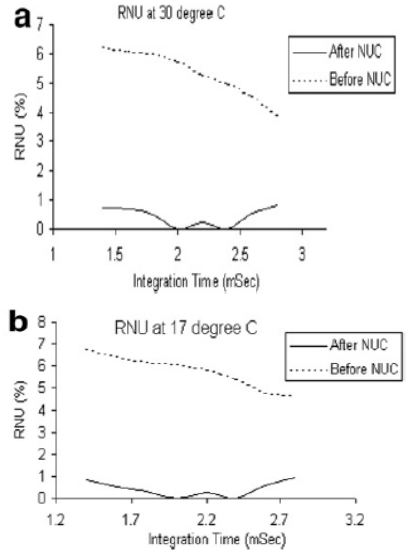

Fig 11 Variation of RNU with integration time at 30 ºC (b) 17 ºC

It can be seen from above figures that the non-uniformities are reduced to approximately 0.6% from 6%. At the

calibration point the residual non-uniformities are minimum and increases as we move away from the calibration point. The spatial non-uniformities are compared with the temporal noise of the system, which is given by standard deviation (SD) (in digital levels). The standard deviation (SD) for the (i,j) th pixel in the FPA is given as:

$$SD = \sqrt{\frac{1}{N_f}\sum_{i=1}^{N_f}(X_{ij} - \bar{X})^2} \qquad (1.23)$$

The temporal mean is given by:

$$\bar{X}_{ij} = \frac{1}{N_f}\sum_{i=1}^{N_f} X_{ij} \qquad (1.24)$$

To determine the temporal noise, 64 frames of image data at each integration time are captured at uniform temperature by exposing the system to a uniform source. This data is used to calculate the SD of each pixel. The frequency distribution then obtained which represents the relationship between the frequency of occurrence and the SD. The maximum value of the distribution gives the temporal noise.

Fig. 12 represents variation of temporal noise and spatial noise after correction with integration time. It can be seen from above figure that spatial noise after non-uniformity correction is less than the temporal noise of the system.

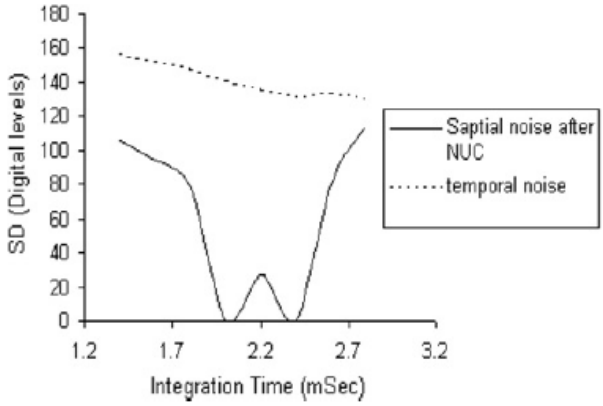

Fig. 12. Variation of temporal and spatial noise with integration time

4. HARDWARE IMPLEMENTATION

The non-uniformity correction algorithm based upon variation of integration time can be easily implemented in hardware.
A scheme for hardware implementation is given in Fig.13

The analog video signal from IRFPA is pre-processed and converted into a digital data using a 14-bit ADC. The 14-bit ADC is used because quantization error should be less than the signal corresponding to the NETD of the sensor array. This raw video digital data, at different integration time, is stored in the frame memory. Serial link is provided to capture the data through PC based application.

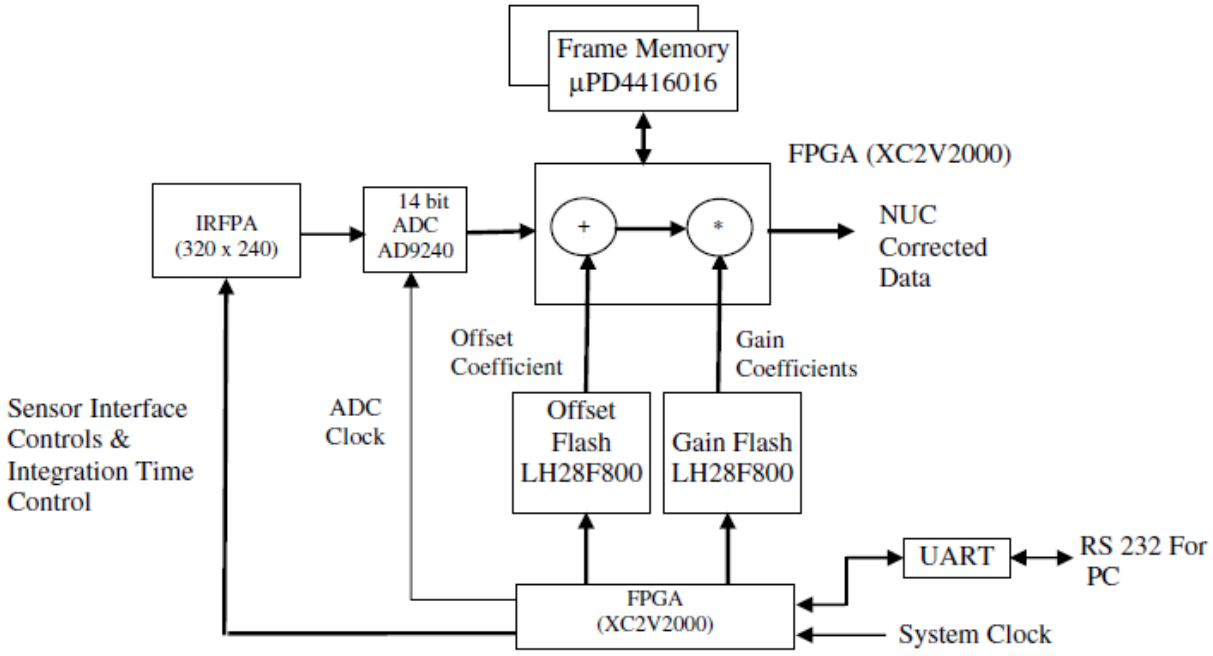

Fig.13 Hardware implementation of the algorithm

Eight frames of raw video data are captured and averaged by successively operating the frame memories in read and write mode. This is done to reduce the temporal noise. The integration time of the IRFPA can be varied through the PC based application and implemented in Xilinx FPGA XC2S2000 based video processing board. The hardware was implemented in VHDL using Xilinx ISE foundation series tool. A snapshot of PC based application is given in Fig.14

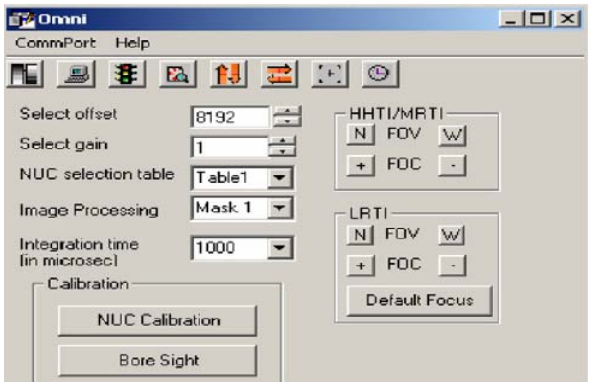

Fig.14 PC based application screen

The gain and the offset coefficients, thus calculated, are stored in offset and gain flash memory. The gain and the offset coefficients are now read from the respective flash and corrections are applied on incoming video data in real time. The data path and the control logic are implemented in a single FPGA. The data path requires only one multiplier and one adder/sub tractor, which can be easily implemented in a FPGA.

5. CONCLUSIONS

A new approach of correcting the sensor non-uniformities is presented. Hardware architecture for implementing the algorithm in real time is given. The results show that residual non-uniformities are reduced from 6% to less that 0.6% after performing the correction. Further, it is observed that the system is fully calibrated at two calibration points. The spatial noise after non-uniformity correction is compared with the temporal noise of the system and the results illustrates that the spatial noise is reduced significantly lower than the temporal noise of the system. This approach offers the sought-after field upgradeability of gain and offset coefficients, thus making the system more robust by giving same performance under all environmental conditions.

REFERENCES

[1] P. Rodriguez, B. Wohlberg, Efficient minimization method for a generalized total variation functional, IEEE Transactions on Image Processing18(2) 322–332, 2009

[2] N. Quacka, Stefan Blunier , Jurg Dual , Martin Arnold , Ferdinand Felder ,Christian Ebneter , Mohamed Rahim, Hans Zog, Vertically moving micro mirror for detectors in the mid infrared Center of Mechanics, ETH Zurich, Switzerland, Sensors and Actuators A 143 29–33, 2008

[3] S. Calderara, R. Cucchiara, A. Prati, Bayesian-competitive consistent labeling for people surveillance, IEEE Transactions on PAMI 30 (2) 354–360. , 2008

[4] N. Jifeng, W. Chengke, L. Shigang, Y. Shuqin, NGVF: an improved external force field for active contour model, Pattern Recognition Letters 28 (1) 58–63, 2007

[5] P. Christol, A. Joullié, Carrier concentration control of GaSb/ GaInAsSb system, Conf. Proc. Am. Inst. Phys. 890 115–124. , 2007

[6] Pedrotti F.L., Pedrotti L.S., & L. M. Pedrotti Introduction to Optics (3rd ed) (pp. 4). New Jersey: Prentice Hall, 2007

[7] Proceedings Vol. 6542 – Infrared Technology and Applications XXXIII, SPIE Defence & Security, Orlando, USA, 2007

[8] R.N. Kacker, J.F. Lawrence, Trapezoidal and triangular distributions for Type B evaluation of standard uncertainty, Metrologia 44(2) 117–127 , 2007

[9] J.W. Little, S.P. Svensson, W.A. Beck, A.C. Goldberg, S.W. Kennerly, T. Hongsmatip, M.Winn, P. Uppal, Thin active region, type II super lattice photodiode arrays: single-pixel and focal plane array characterization, J. Appl. Phys. 101 044514.1–044514.6. , 2007

[10] M. De Flumere, H. Stewart, W. Watson, Modeling of type II Super lattice photodiodes, in: Infrared Technology and Applications XXXIII, Proceedings of SPIE, vol. 6542, 2007

[11] S. Lim, A. El Gamal, "Gain FPN Correction via Optical Flow", IEEE Transactions on Circuits and Systems I: Regular Papers, vol. 51, no. 4, APRIL 2004.

[12] Xavier N. Fernando, Sridar Krishnan, Hongbo Sun and Kamyar Kazemi-Moud Adaptive denoising at Infrared wireless receivers, , Department of Electrical and Computer Engineering, Ryerson University Toronto, ON, M5B, Canada, 2003

[13] Math works Corp., "MATLAB Technical Computing Environment," www.mathworks.com, Jan. 2003

[14] M. Elad, "On the origin of the bilateral filter and ways to improve it," IEEE Trans. Image Process., Oct. 2002, vol. 11, no. 10, pp. 1141–1151, 2002

[15] Mehra J., Rechenberg H. The historical development of quantum theory: Volume 1, part 1, Springer 2001

[16] Norton P., Campbell J. and Horn S., "Third generation infrared imagers," Infrared technology and applications XXVI, Proceedings of SPIE, Vol. 4130, pp. 226-236, 2000.

[17] Martens J.B., "Adaptive contrast enhancement through residue image processing," Signal Processing, Vol. 44, pp. 1-18, 1995.

[18] Martens J.B., "Noise reduction and enhancement by mean of adaptive residue image processing," IEEE Conference on Image Processing (ICIP-94), pp. 467-471, 1994.